The Astronomical Journal, 148:5 (9pp), 2014 July doi:10.1088/0004-6256/148/1/5

THE SPIRAL ARMS OF THE MILKY WAY: THE RELATIVE LOCATION OF EACH DIFFERENT ARM TRACER WITHIN A TYPICAL SPIRAL ARM WIDTH

Jacques P. Vallée
National Research Council Canada, National Science Infrastructure portfolio, Herzberg Astronomy and Astrophysics,
5071 West Saanich Road, Victoria, B.C., V9E 2E7, Canada; jacques.vallee@nrc-cnrc.gc.ca
Received 2013 July 5; accepted 2014 April 19; published 2014 May 23

ABSTRACT

From the Sun's location in the Galactic disk, different arm tracers (CO, H I, hot dust, etc.) have been employed to locate a tangent to each spiral arm. Using all various and different observed spiral arm tracers (as published elsewhere), we embark on a new goal, namely the statistical analysis of these published data (data mining) to statistically compute the mean location of each spiral arm tracer. We show for a typical arm cross-cut, a separation of 400 pc between the mid-arm and the dust lane (at the inner edge of the arm, toward the Galactic center). Are some arms major and others minor? Separating arms into two sets, as suggested by some, we find the same arm widths between the two sets. Our interpretation is that we live in a multiple (four-arm) spiral (logarithmic) pattern (around a pitch angle of 12°) for the stars and gas in the Milky Way, with a sizable interarm separation (around 3 kpc) at the Sun's location and the same arm width for each arm (near 400 pc from mid-arm to dust lane).

Key words: galaxies: individual (Milky Way) – ISM: general

Online-only material: color figures

1. INTRODUCTION

There have been numerous published results for the spiral arms of the Milky Way. With the Sun in the Milky Way disk, the majority of published observational results have focused on different parts of our Galaxy. For statistical purposes, we embarked on a series of papers covering the period 1980 onward, cataloging results as tabulated in blocks of 15–20 each: Vallée (1995, 2002, 2005, 2008, 2013; papers I–V). This one (paper VI) presents and analyzes the latest blocks.

The overall value of the data summarized here is to view them in a general context, conducive to a standardized tabulation, and some statistics to be done with time.

As usual, we employ all recent research in this area, use a "relative weight" for statistics, and attempt a reconstruction of the results in order to present a Galactic view. The relative weight attempts to take account of biases such as the neglect of dust patches that would suggest a more distant object, the neglect of corrective terms in proper motions that would suggest a closer object, or the neglect of a positive or negative velocity shock jump in kinematical distances that would yield a different distance. Section 2 of this paper presents the latest results, garnered from published spiral arm research obtained since 2012.

Here, we investigate the relative position of each arm tracer in each arm, from the angular distance between an arm tangent (tracer X) and the mid-arm position. This is a first for our Milky Way galaxy, but it has been found in some other nearby galaxies. Section 3 computes a sketch of a typical arm width using different arm tracers (CO, H I, hot dust, masers, etc.). Section 4 splits the known spiral arms into two sets and compares their widths. Some conclusions and comparisons are carried in Section 5.

2. RECENT DATA

Here, we attempt to analyze and evaluate and then assign a value (1, 2, 3, with best = 3) to some recently published results (data). A low weight (1) is given to dust-affected measurements, with potentially incomplete corrections due to irregular dust patches impacting the distance determinations; some optical appearances may be affected by an uneven angular distribution of dust reddening or interstellar extinction. A top weight (3) is given for simple methods with the least number of assumptions, such as the parallax or the arm tangents. A medium weight (2) is given to all other methods, notably radial-velocity-based methods that are also potentially affected by velocity jumps in shocked gas, while some imprecisions remain in the LSR velocity for the Sun.

We summarize the results extracted from studies on the spiral arms in the Milky Way since early 2012 (Table 1) and 2013 so far (Table 2). We average across all methods in the last rows of Tables 1 and 2.

Qualitative comments are given in the Appendix on some recent results, where appropriate.

3. DATA MINING AND NEW STATISTICS—CROSS-CUT OF AN ARM WIDTH

Data for the longitudes of each arm tracer have been published elsewhere. A compilation was provided in Vallée (2008). Since then, one can add the arm tangents as inferred from the recent 6.7 GHz methanol masers data (Pandian & Goldsmith 2007; Caswell et al. 2011; Green et al. 2011).

Using published data in refereed journals, here we investigate a new goal: to find the relative positioning of each arm tracer, from the angular distance between an arm tangent (tracer X) and the mid-arm position, using the power of statistics. Just like stacking plates, to eliminate noise (positive and negative) and to enhance a true signal (positive), we wish to add the signal from each spiral arm coming from a given tracer.

We used the tangent interpretation as published in the original paper, with the intensity as a function of longitude. We did not attempt here to reinterpret the original intensity data to get a different tangential longitude. We believe that statistical analysis

Table 1
Recent Studies of Spiral Arms in the Milky Way (2012)

Pitch Angle (deg)	No. of Arms	Arm Shape[a] $\varphi = f(r)$	Inter arm[b] (kpc)	Relat. Wgt (3 = best)	Data Used ...	Figures and References ...
11°	4	log	3.7	2	CO; kinematical	Figure 1(b) in Dobbs & Burkert (2012)
15°	4	log	2.8[c]	3	Maser astrometry	Figure 1 in Honma et al. (2012)
6.0	2	log	2.2[c]	1	Star clusters	Figure 6 in Kharchenko et al. (2012)
5.6	2	log	2.2[c]	1	Local disk stars	Figure 7 in Francis & Anderson (2012)
15°	4	log	3.4[c]	2	Young stellar object; CO	Figure 4 in Moore et al. (2012)
12.5°	4	log	3.1[c]	2	Near IR; mid-IR stars	Figure 10 in Robitaille et al. (2012)
05°	4	log	...	1	*ubvy* of stars	Figure 7(a) in Kaltcheva & Golev (2012)
15°	4	log	3.7[c]	3	OH masers	Figure 6 in Green et al. (2012)
12°	4	log	2.8[c]	3	Pulsars; free electron	Figure 1(b) in Schnitzeler (2012)
10°	2	wave	2.2	1	Local stars	Figure 4(b) in Siebert et al. (2012)
15°	4	log	3.4	1	Open star clusters	Figure 20 in Camargo et al. (2012)
12°	4	log	...	1	H II regions, with H I abs	Figure 7 in Jones & Dickey (2012)
12°	4	log	3.3[c]	1	H II regions with HI abs	Figure 8 in Urquhart et al. (2012)
12°	4	log	2.9	2	X-ray binaries	Figure 2 in Bodaghee et al. (2012)
12°	4	log	...	1	C II 158μ Scutum	Figure 1 in Velusamy et al. (2012)
12°	4	log	2.8[c]	2	6.7 GHz methanol masers	Figure 1 in Matsumoto & Honma (2012)
12°	4	log	2.6	2	Cosmic-ray protons energy	Figure 1 in Effenberger et al. (2012)
12.0	4	log	2.9	...	Median value (all data)	
11.4	...	log	3.0	...	Unweighted mean (all data)	
±0.9	...	...	±0.2	...	Standard deviation of the mean (all data)	

Notes.
[a] $\varphi = f(r)$ means the azimuthal angle φ follows a function of the radius r of the form f, where f is usually logarithmic, or if not, then polynomial or complex or ring.
[b] Distance between Perseus arm and Sagittarius arm, near the Sun's location.
[c] Corrected by assuming 8.0 kpc for the Sun–GC distance (not the 8.5 or else as used).

Table 2
Recent Studies of Spiral Arms in the Milky Way (2013)

Pitch Angle (deg)	No. of Arms	Arm Shape[a] $\varphi = f(r)$	Inter arm[b] (kpc)	Relat. Wgt (3 = best)	Data Used ...	Figures and References ...
12.8	4	log	2.7	2	Runaway stars	Figure 9 in Silva & Napiwotski (2013)
12.7	4	log	2.6	2	CO, molecular clouds	Figure 2 in Eden et al. (2013)
14°	4	log	3.3[c]	3	Water masers	Figure 10(a) in Xu et al. (2013)
15°	4	log	3.8[c]	2	Dust continuum; kinematical	Figure 10 in Ellsworth-Bowers et al. (2013)
15°	4	log	3.3	1	Open star clusters	Figure 14 in Camargo et al. (2013)
12°	4	log	3.6	1	Detached eclipsing binaries	Figure B1 in Helminiak et al. (2013)
12°	4	log	3.5[c]	1	6.7 GHz methanols	Figure 18 in Urquhart et al. (2013)
12°	4	log	3.0	2	Open star clusters	Figure 7 in Chené et al. (2013)
6°	2	log	5.3	1	Cepheid kinematics	Table 1 in Griv et al. (2013)
10°	4	log	3.2[c]	2	Pulsars	Figure 1 in Han (2013)
12°	4	log	3.3[c]	2	Pulsars	Figure 3 in Nice et al. (2013)
12°	4	log	...	1	CBe stars	Figure 11 in Raddi et al. (2013)
14°	multiple	log	1.0[d]	1	Cepheids, open star clusters	Figure 9 in Junqueira et al. (2013)
13.5	4	log	3.4	2	N II 205 μm	Figure 2 in Higdon & Lingenfelter (2013)
9.5	4	log	3.4[c]	3	22 GHz water masers	Figure 11 in Zhang et al. (2013)
12.0	4	log	3.3	...	Median value (all data)	
12.2	...	log	3.2	...	Unweighted mean (all data)	
±0.6	...	...	±0.2	...	Standard deviation of the mean (all data)	

Notes.
[a] $\varphi = f(r)$ means the azimuthal angle φ follows a function of the radius r of the form f, where f is usually logarithmic, or if not, then polynomial or complex or ring.
[b] Distance between Perseus arm and Sagittarius arm, near the Sun's location.
[c] Corrected by assuming 8.0 kpc for the Sun–GC distance (not the 8.5 or else as used).
[d] There are multiple gas-response arms (top red curve to top green curve), aka short arms.

Table 3
Computed Distance of Each Tangent Arm Tracer, from the Mid-arm Location

Name	Tracer	Arm Tangent[a]	Angular Distance[b]	Linear Separation from ^{12}CO Tangent
Carina	^{12}CO	282°	0°	0 pc, with this arm at 5 kpc from Sun[c]
	Thermal electron	283°	1°	87 pc
	H II complex	284°	2°	174 pc
	Dust 60μ	285°	3°	262 pc
Crux	^{12}CO	308°	0°	0 pc, with this arm at 6 kpc from Sun[c]
	Thermal electron	309°	1°	105 pc
	H II complex	309°	1°	105 pc
	H I atom	310°	2°	209 pc
	^{26}Al	310°	2°	209 pc
	Synch. 408 MHz	310°	2°	209 pc
	Dust 60 μm	311°	3°	314 pc
Norma	H II complex	323°	−5°	−610 pc
	^{26}Al	325°	−3°	−366 pc
	^{12}CO	328°	0°	0 pc, with this arm at 7 kpc from Sun[c]
	Thermal electron	328°	0°	0 pc
	H I atom	328°	0°	0 pc
	Synch. 408 MHz	328°	0°	0 pc
	Dust 60 μm	329°	1°	122 pc
	Methanol masers[d]	331.°5	3.°5	427 pc
	Dust 2.4 μm	332°	4°	488 pc
Start of Perseus	^{12}CO	336°	0°	0 pc, with this arm at 8 kpc from Sun[c]
	Methanol masers[e]	338°	2°	279 pc
	Dust 2.4 μm	339°	3°	419 pc
	Synch. 408 MHz	339°	3°	419 pc
	Dust 60 μm	340°	4°	558 pc
Scutum	^{12}CO	033°	0°	0 pc, with this arm at 5 kpc from Sun[c]
	Synch. 408 MHz	032°	1°	87 pc
	^{26}Al	032°	1°	87 pc
	Thermal electron	032°	1°	87 pc
	^{13}CO	032°	1°	87 pc
	H II complex	032°	1°	87 pc
	H I atom	029°	4°	349 pc
	Dust 2.4 μm	029°	4°	349 pc
	Methanol masers[e]	026°	7°	609 pc
	Dust 60 μm	026°	7°	609 pc
Sagittarius	H II complex	056°	−1°	−70 pc
	^{12}CO	055°	0°	0 pc, with this arm at 4 kpc from Sun[c]
	^{13}CO	052°	3°	209 pc
	H I atom	050°	5°	349 pc
	Methanol masers[f]	49.6°	5.4°	376 pc
	Thermal electron	049°	6°	418 pc
	Synch. 408 MHz	048°	7°	487 pc
	^{26}Al	046°	9°	626 pc

Notes.
[a] Observed arm tangents are read from Table 2 in Vallée (2008), except for recent methanol masers. The CO tracer is taken as representing the mid-arm. This CO tracer is the low-excitation $J = 1$–0, low temperature (∼10 K), low-angular resolution (∼9 arcmin), narrow line width (∼2 km s^{-1}), 115 GHz data from the Columbia survey, as integrated over a velocity range associated with a spiral arm (Bronfman 2008, 1992; Grabelsky et al. 1988).
[b] Angular separation is positive toward inner arm edge (Galactic center); negative toward outer arm edge (outer Galaxy).
[c] Distance from Sun to each arm is from Figure 2 here, and computed using 8.0 kpc for the Sun–Galactic center distance.
[d] Caswell et al. (2011).
[e] Green et al. (2011).
[f] Pandian & Goldsmith (2007).

will take care of minor random errors from one published study to the next.

Different arm tracers appear at different Galactic longitudes. To transfer angular to linear offsets, we used the canonical four-arm logarithmic spiral model, with a Sun–Galactic center distance of 8.0 kpc.

Table 3 shows the angular and linear separation of each individual arm tracer from the mid-arm (from the longitude of arm tangent for tracer X versus the longitude of ^{12}CO arm tangent).

As we seek the inner edge of spiral arms, the dust tracers in Table 3 are observed at higher Galactic longitudes in the fourth quadrant (longitudes 270°–360°) but at lower Galactic longitudes in the first quadrant (longitude 0°–90°).

It can be seen that the hot dust arm tangents (and the methanol masers) are always inward, closer to the Galactic center.

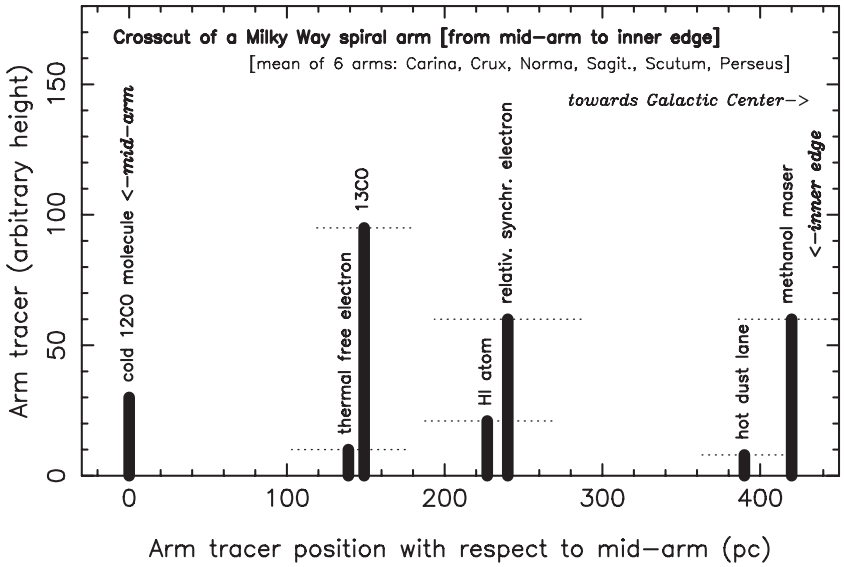

Figure 1. Sketch of a cross-cut of a typical spiral arm in the Milky Way, averaged over six arms. This sketch indicates the mean position of each spiral arm tracer within an arm, from the mid-arm (^{12}CO arm tangent, at 0 pc) to the inner arm edge (hot dust tangent, near 400 pc). The direction toward the Galactic center is to the right. Mean data are from Table 4; original data are from the individual arm tangents in Table 3. Here, the relativistic electron is the synchrotron—408 MHz emission used as an arm tracer. The sdm is noted as a horizontal dotted line, for each arm tracer.

Table 4
Statistics on Linear Separation[a] for Each Arm Tracer, for the Milky Way's Arms

	Sagit. (pc)	Carina (pc)	Norma (pc)	Start of Perseus (pc)	Scutum (pc)	Crux (pc)	Mean Separation (pc)	sdm (pc)
^{12}CO	0	0	0	0	0	0	0	0
H II complex	−70	174	−610	...	87	105	−63	142
Thermal electron	418	87	0	...	87	105	139	72
^{13}CO	209	...	...	...	87	...	148	61
^{26}Al	626	...	−366	...	87	209	139	204
H I atom	349	...	0	...	349	209	227	82
Synch. 408 MHz	487	...	0	419	87	209	240	93
Methanol masers	376	...	427	279	609	...	422	69
Dust 60 μm	...	262	122	558	609	314	373[b]	92[b]
Dust 2.4 μm	...	...	488	419	349	...	419[b]	40[b]

Notes.
[a] All data from Table 2 here. Separation is from the CO arm tangent.
[b] Stats made on both dust tracers together give a mean separation of 390 pc, with sdm of 57 pc.

Interesting statistics can be had by summing and averaging over all spiral arms. Thus, we could determine if arm tracers have separate lanes and, if so, where are they observed in the Milky Way. Separate lanes between different arm tracers were predicted by various galactic theories.

Table 4 pulls together the statistics over six spiral arms in the Milky Way, indicating the mean separation for each arm tracer, from the mid-arm. The uncertainties of the centroid are given for each tracer as horizontal bars.

A net separation can be found here for some of the arm tracers, notably for CO (large beam), thermal electrons (galactic free electrons, from pulsar rotation measure and dispersion measure), relativistic electrons (408 MHz synchrotron), hot dust (60 μm and 2.4 μm together), and methanol masers (6.7 GHz).

Figure 1 shows a cross-cut of a spiral arm, showing the position of a typical arm tracer with respect to the mid-arm, for the Milky Way (mean data from Table 4). Six arms were used for this cross-cut. The direction to the Galactic center is to the right. It is interesting that the hot dust lane (60 μm and 2.4 μm arm tangents) is always to the right of the ^{12}CO arm tangents, while the relativistic electron (408 MHz arm tangents) is always in between the mid-arm and dust lane.

The observed half width of a typical arm (400 pc from mid-arm to the inner edge) can be doubled in order to get the full arm width, giving about 800 pc. The standard deviation of the mean (sdm) is given for each arm tracer with the horizontal dotted lines. The mean sdm observed for the arm tracers shown (excluding ^{12}CO) is 73 pc, only about 10% of the full arm width of 800 pc.

In the Milky Way, Higdon & Lingenfelter (2013) found that an interarm contribution to the 205 μm N II emission is not required, when using a "half-arm width" of 0.5 ± 0.1 kpc for the emission from the four spiral arms and two very nearby sources (Cygnus X and Gum–Vela Complex). *Had they allowed for a small interarm contribution to N II, then they would have had to take a smaller half-arm width.*

Our interpretation is that a typical Milky Way spiral arm shows a different location for each arm tracer, from CO (mid-arm) until hot dust (inner arm), with a half-width arm of about 400 pc.

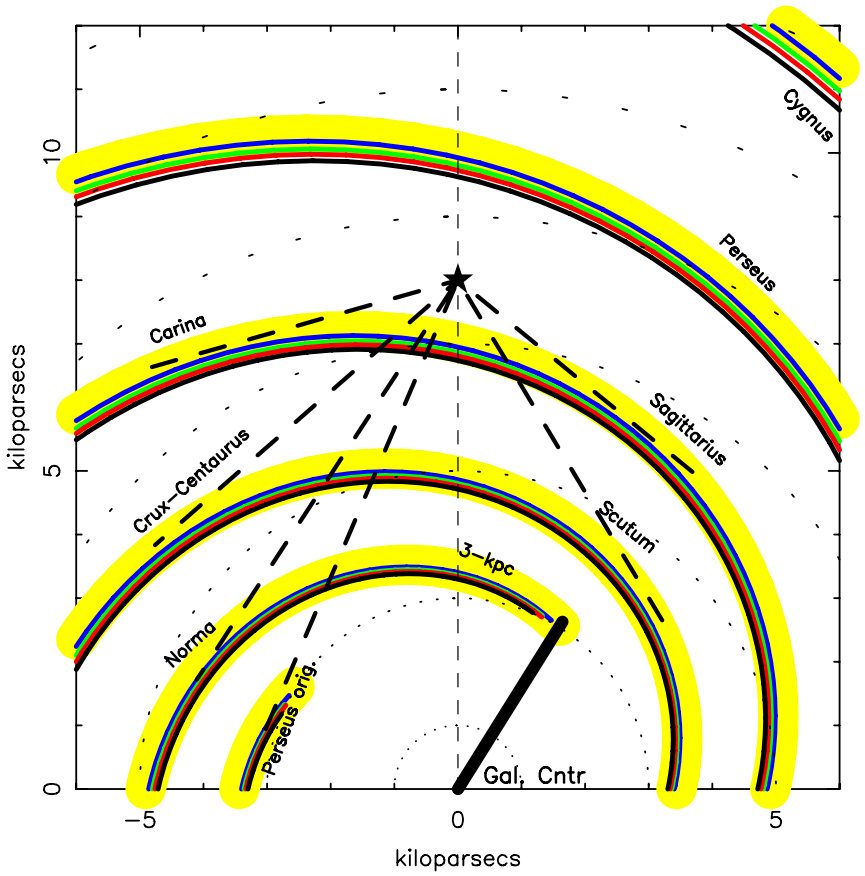

Figure 2. Sketch of a four-arm model, with a 12.°8 pitch angle. Different arm tracers are shown in different colors: CO tracers are shown in yellow; free thermal electron tracers are shown in green; synchrotron relativistic electron tracers are shown in green; hot dust tracers are shown in red; methanol maser tracers are shown in black. The width of each lane shown here is arbitrary, to prevent overlap (the true centroid and its error can be read in Table 4). The Sun is shown at (0.0, 8.0) as a star. Circular paths around the Galactic center are shown as black dotted circles at various Galactic radii; these paths roughly represent clockwise orbital motions of stars and gas clouds, coming from the left then entering the inner edge of a spiral arm, being compressed, then continuing inside the arm and exiting at the outer arm edge. Dashed lines from the Sun (star) show locations of some arm tangents.

(A color version of this figure is available in the online journal.)

Error analysis. We used the published longitude of the arm tangents for CO as our fiducial mark in each arm (zero in horizontal axis in Figure 1, zero angular distance in Table 3). However, we could have used the median longitude of all tracers (CO, dust, etc.) as our fiducial mark in each arm. This turned out to give a small error bar to the location of CO relative to the median of all tracers. Thus, we found an offset of −2.°5 for the CO from the median of all tracers, with a standard error of the mean of 0.°7 or 88 pc for the CO tangent. However, the overall results were the same (CO always being seen to the left of the median longitude of all tracers in the arm cross-cut, dust always being to the right of the median longitude in the arm cross-cut), with the same half-arm width of about 400 pc. Thus, the relative error in the CO position over a full arm width is 88/800 or 11%.

For the Carina arm, there is agreement within the errors for the CO tangent to be at longitude 282° (Bronfman 1992) or very nearby at 281° (Grabelsky et al. 1988); both are offset from the mean of all tracers near 284° (Vallée 2008).

Arm analysis. The majority of published papers favor a four-arm spiral model, with a mean pitch angle near 12°. Figure 2 shows a sketch of a four-arm spiral model, using the arm parameters from Tables 1 and 2 and in earlier papers in this series. The observational tangents are shown as dashed lines darting from the Sun (from Table 2 in Paper IV). There is no "molecular ring," but a region encompassing the origins of four spiral arms (Section 3.2 in Paper IV), as supported more recently by Dobbs & Burkert (2012). Inputs are a pitch angle $p = 12.°8$, $m = 4$ arms, logarithmic shape, and $R_{\rm Sun} = 8.0$ kpc. Outputs are an interarm near 3 kpc, a distance to W3(OH) near 2 kpc, and a fit to the six observed mean arm tangents. Because of the large pitch angle, none of these arms can turn around a full circle within the Sun's position. There are three arms seen in Figure 2 between a Galactic radius of 3.5 and 7.5 kpc, giving a mean mid-arm to mid-arm separation of 2000 pc, thus about 2.5 full arm widths.

Dynamically, the kinematical appearances of the arms in a four-arm *spiral* model was shown elsewhere (Vallée 2008; his Figure 3). Stars enter and leave the arms in their quasi-circular dynamical orbits around the Galactic center (adapted from Roberts 1975). Outside the arms, the Galactic orbits for gas in the gravitational potential were likened to a "4-segment spiral" (Vallée 2011; his Figure 37).

We have drawn the central bar at a canonical value. Lopez-Corredoira et al. (2007) gave a history of this structure. Recent methanol maser data puts it at an angle of 45°, ending near the origins of some spiral arms: Galactic longitude 352° is the start of the Sagittarius arm, and Galactic longitude 12° is the start of the Norma −3 kpc arm, according to Green et al. (2011). These arm origins are points, but they are not arm tangents. Note that

Table 5
Differences Between Two Sets of Spiral Arms in the Milky Way

	Set A[a] Mean Separation from CO Tangent	sdm	Set B[b] Mean Separation from CO Tangent	sdm	Differ.: Set A − Set B	sdm	Comment
^{12}CO	0	0	0	0	0	0	As set
Thermal electron	168	128	96	9	+72	128	Less than 1 sigma
^{13}CO	209	...	87	...	+122	...	Unknown sigma
H I atom	174	174	279	70	−132	199	Less than 1 sigma
Synch. 408 MHz	244	243	238	97	+6	262	Less than 1 sigma
Methanol masers	401	25	444	165	−43	167	Less than 1 sigma
Dust 60 μm	192	70	494	91	−302	115	Less than 3 sigmas
Dust 2.4 μm	488	...	384	35	+104	...	Unknown sigma
All dust	291	107	450	58	−159	122	only 1.3 sigmas
					−37	46	Overall mean difference

Notes.
[a] All individual data from Table 3 here; without tracers having too few data.
[b] Set A is composed of Sagittarius, Carina, Norma arms (Columns 2–4 of Table 4); set B is composed of Scutum, Crux, Start of Perseus (Columns 5–7 of Table 4).

the longitude of an arm origin cannot be located at the longitude of the tangent to that arm as seen from the Sun.

As pointed out by Dame & Thaddeus (2008), the existence of tangents to the "near 3 kpc arm" is still in doubt, but they assumed them to be $+23^\circ$ and -23° (aka -337°). From Tables 3 and 4, here the -23° is accepted and renamed the "Start of the Perseus arm," while the $+23^\circ$ has not been confirmed with at least four different arm tracers (hence this longitude is probably not a tangent). In our Figure 2 this arm has an origin near longitude 16° (an origin is a point, not an arm tangent). The "far 3 kpc arm," as seen in Figure 1 of Dame & Thaddeus (2008) with distance near 12 kpc and radial velocity near $+56$ km s^{-1} at longitude 0° (their Table 1), does not show its arm tangents.

The continuation of the Scutum–Centaurus–Crux arm behind the Galactic center was observed by Dame & Thaddeus (2011), who located it at a mean distance of 21 kpc, a mean longitude of $+34^\circ$, and a mean radial velocity of -52 km s^{-1} (their Figure 1). No arm tangents to this arm are shown (their Figure 4).

4. APPLICATIONS

Some authors upgrade two spiral arms and downgrade two other arms, calling them "major" and "minor."

Is Sagittarius major? (a) CO and ^{13}CO: the nearby spiral arm, Sagittarius, is known to possess clearly observed extended structures in Galactic longitudes as well as long arcs in longitude–velocity plots of ^{12}CO and ^{13}CO line emissions (Sawada et al. 2012; Figure 5 in Roman-Duval et al. 2010). Its appearance at longitudes $>180^\circ$ (renamed the Carina arm) is "major" in molecular gas (Figure 4 in Grabelsky et al. 1988). (b) CS and NH_3: Urquhart et al. (2014) studied young massive stars through these spectral lines and found the Sagittarius arm to be more prominent than the Perseus arm, suggesting that the Sagittarius arm is a major feature of the Galaxy as traced by massive star formation (their Section 4.1.3). (c) NIR: Steiman-Cameron et al. (2010) noted that the Sagittarius arm is seen in every major tracer and its existence as a "major" arm is not in question; they pointed to unusual absorption, enhanced significant and excessive obscuration, and increased extinction, in the near infrared toward and around the W51 complex near the tangential arm direction (their Section 4.1). (d) Optical data using Cepheid stars suggests that the Sagittarius arm is a "major" arm (Figure 7 in Majaess et al. 2009). Given the huge amount of molecular gas in the Sagittarius–Carina arm, and using a typical gas-to-dust mass ratio, one would expect a huge amount of dust there, capable of severely hindering star counts in that arm (as reported in the optical or near-infrared regime).

Therefore, in an alternating major–minor arm model, with Sagittarius as "major," the adjacent Perseus arm would be termed a "minor" arm. Zhang et al. (2013) found a 6 kpc gap in the Perseus arm, without star formation (between $50^\circ <$ longitude $< 80^\circ$), so Perseus would be a "minor" arm in that arm segment. If the segment seen from the Sun is representative, then the whole Perseus arm is "minor" and the adjacent Sagittarius arm is "major."

Is Sagittarius minor? Alternatively, some near-infrared stellar counts seem to suggest that the Perseus arm and the Scutum arm are "major" arms (e.g., Robitaille et al. 2012: Siebert et al. 2012), while the other two adjacent arms (including Sagittarius) are termed "minor" arms.

Thus, the adjacent Sagittarius arm and Perseus arm would be "major" and "minor" in different tracers or in some arm segments, if using a model with adjacent major and minor arms.

A look at the arm widths could shed some information here. Which set of arms is "major" and which set of arms is "minor"?

Table 5 does the same as for Table 4, except that the arms are separated into two sets: set A is composed of Sagittarius, Carina, and Norma arms. Set B is composed of Scutum, Crux, and start of Perseus arm. The statistics of Table 4 are repeated in Table 5 for each of the two sets and the difference for each arm tracer is computed. One can see that the differences between the two sets are almost evenly distributed between the nine different arm tracers (four +, four –, and one 0). This Table 5 does not support the notion that the two sets of arms are different in arm widths.

The bottom of Table 5 shows the overall mean difference between the two sets, being -37 with an sdm of 46. The chance probability that the two sets significantly differ is practically zero. From the arm widths, neither set A nor B can pretend to be "major" or "minor," as both reveal equal widths (from CO to hot dust lane).

Figure 3 does the same as Figure 1, where set A (in red) is compared to set B (in blue). The data come from Table 5.

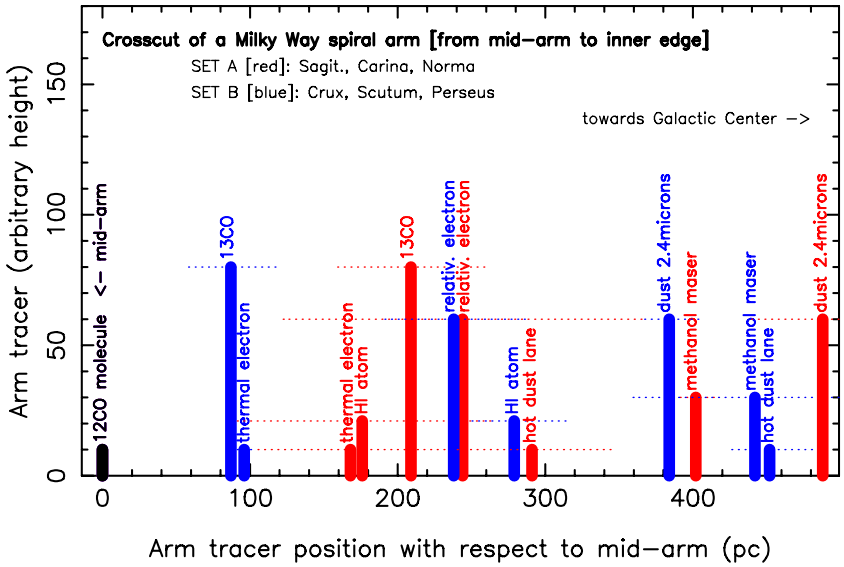

Figure 3. Sketch of cross-cut of a typical spiral arm in the Milky Way, done separately for set A (three arms) and for set B (three arms). This sketch indicates the mean position of each spiral arm tracer within an arm, from the mid-arm (^{12}CO arm tangent, at 0 pc) to the inner arm edge (hot dust tangent, near 400 pc). The direction toward the Galactic center is to the right. Mean data are from Table 5.

(A color version of this figure is available in the online journal.)

The thermal electron data and ^{13}CO data for set B are closer to ^{12}CO, but the H I atom data and hot dust lane data for set A is closer to ^{12}CO. The relativistic electron data are virtually at the same distance from ^{12}CO. The methanol maser data for set A are virtually at the same distance as for set B. Different dust data for set A extend from 291 to 488 pc, while for set B they extend from 384 to 450 pc.

Thus, we conclude that there is no visually significant statistical separation between the arm width of set A and that of set B. Comparing the two sets A and B, one finds an arm width ratio of around 1.0.

5. CONCLUSION

Recent data on the Milky Way's spiral arms since early 2012 using different arm tracers are classified, statistically analyzed, and presented as a reconstruction of a Galactic map. Our analysis for the recent data (Tables 1 and 2) favors a model with a four-arm spiral pattern and an interarm separation at the Sun's location near 3 kpc.

We provide a sketch of a cross-cut across a spiral arm, indicating the mean position of a spiral arm tracer with respect to the mid-arm, for the Milky Way (Figures 1 and 2; Tables 3 and 4). Linear offsets between different arm tracers were predicted by various theories of spiral arms, as well as observed in other spiral galaxies (see a recent review in Louie et al. 2013). We found for the Milky Way that each spiral arm tracer can occupy a separate lane *across* an arm. This is the first time it is found in the Milky Way galaxy, owing to the Sun's position in the Galactic disk.

Looking at another spiral galaxy, face-on, and focusing on one of its arms, one often finds an arm segment here and there without much stellar content, bracketed by other segments with more stars, along the same spiral arm. It was found elsewhere that differing "segments" can be found *along* an arm; some segments may have more stars while others may have more gas. Thus, if we "move" the Sun at different positions (segments) in the same arm, we may see different local views in optical (star), near infrared (dust), or radio (relativistic electrons, molecular gas). Yet the local view from the Sun can easily miss an arm segment when using a single filter (only CO data, or only stellar counts). There are many calibration issues when using a single arm tracer. The Sun's location and its view of nearby arm segments could give the wrong impression of two "major" arms and two "minor" arms.

Separating arms into two sets (Table 5 and Figure 3) does not support a model with alternating "major" and "minor" arms. Thus, the methanol masers and the hot dust lane are always near 400 pc from the mid-arm, in both the spiral arms called "major" and those called "minor."

Hurt (http://www.spitzer.caltech.edu/images/1925-ssc2008-10b-A-Roadmap-to-the-Milky-Way-Annotated-) produced a color drawing of the Milky Way that has been used widely by researchers. His color drawing shows two "major" spiral arms and two "minor" spiral arms. In his color picture, the arm width is tiny for his "minor arms" (aka set A above) and the arm width is huge for his "major arms" (aka set B above). Reading from Hurt's drawing, one finds an arm width of about 1500 pc for his major arms and about 600 pc for his minor arms. Thus, comparing his "major" versus "minor" arms, there is an arm width ratio of 2.5 between the two sets (contrary to our findings above). Other issues with Hurt's drawing have been cataloged elsewhere (see the list at http://galaxymap.org).

Sky surveys indicate that a sizable minority of galaxies possess a four-armed spiral with a bar; notable look-alike Milky Way galaxies include UGC 06155, NGC 5970, NGC 0180, NGC 3346, and NGC 6744 (see some color images at www.galaxyzooforum.org)

The figure production made use of the PGPLOT software at the NRC-nsip in Victoria. I thank the referee for helpful comments. Each year brings a lot of new papers on this topic; recent preprints (arXiv, etc.) will be processed in the next paper in this series (in preparation).

APPENDIX

Qualitative comments are given below on some recent results, where appropriate.

Kharchenko et al. (2012) used a two-arm spiral model with a low pitch angle (from Piskunov et al. 2006); this model has many turns around the Galactic center before reaching the Sun, and thus many unproven tangents to the arm segments.

Francis & Anderson (2012) used light intensity from the 2 μm All Sky Survey catalog, and suggested a two-arm spiral model, with a low pitch angle, predicting 11 tangents to the arms toward the Galactic center, namely at longitudes 260°, 308°, 322°, 333°, 340°, 343°, 016°, 022°, 030°, 042°, and 080°. Their two-arm model places the Sun pretty much in the Perseus arm (at about 200 pc), but maser measurements of H II regions in that arm near longitude 130° put the masers at 2 kpc away. Also, their model tangent to the nearby Sagittarius arm at longitude 042° differs substantially by 9° from the observed tangent at 051° when using seven different observed arm tracers. We suggest that an intensity peak may either indicate (1) a real physical arm tangent (stars aligned in a tube along the line-of-sight) or (2) a false arm tangent (a compact spherical star cluster, not along a tube along the line of sight).

Kaltcheva & Golev (2012) used *ubvy* color data from stars in open clusters to investigate the Galactic structure near the Carina spiral arm. Points taken along their model fit (their Figure 7(a)) were translated into distances (using data from their Table 2) and plotted on the Galactic disk (at their proper longitudes), from which a mean pitch angle was obtained here.

Siebert et al. (2012) studied over 213,000 stars within 2 kpc of the Sun in the disk and within 1 kpc from the disk and fitted a density wave model under the assumption of long-lived spiral arms being long-lived density waves. Using 8 kpc as the distance of the Sun to the Galactic center, their preferred models showed the Sagittarius arm "merging" with the Perseus arm at 3 kpc away from the Sun near a Galactic longitude of 90° (their Figure 4(b)), with a small interarm Perseus–Sagittarius distance of 2.2 kpc, and the peak of the Scutum arm being only 2.7 kpc from the Sun toward longitude 0°.

Dobbs & Burkert (2012) fitted spiral and ring models to the CO data, found the best statistical fit to be for the four-arm model (their Table 1), and concluded that "reproducing all the features in the CO" required four spiral arms (their Section 4). In addition, they argued that the so-called "molecular ring" near 4 kpc from the Galactic center is not a true physical ring, but one segment of a long spiral arm with additional segments from other spiral arms. A similar conclusion was presented in Vallée (2008; his Section 3.2).

Robitaille et al. (2012) used near- and mid-infrared data (essentially stellar and dust emission) to model the spiral arms, increasing the O-type and B-type stellar populations in the Scutum arm and Perseus arm by a factor of two and thus create two "major" arms and two "minor" arms.

In Table 1 of Griv et al. (2013), the relative χ^2 estimator (merit function) is very close for the two-arm and four-arm structures (143 versus 145), at most a 2% difference. Nearby Cepheids were selected, out to a maximum distance of 4.1 kpc from the Sun.

In matching the 205 μm N II emission, Higdon & Lingenfelter (2013) had to (1) decrease by a factor two the parameter f of the Norma–Cygnus and the Sagittarius–Carina arms; and (2) insert two very nearby sources in the local spur, a 6°-sized Cygnus X at l, b = (80°, 0°) at 1.45 kpc, and a 10°-sized Gum–Vela Complex at l, b = (262°, −2°) at 0.33 kpc.

Junqueira et al. (2013) employed a two arm imposed perturbed gravitational potential to generate multiple stellar orbits and bifurcations that appear as short stellar/gas arms near the Sun. Thus, the Perseus arm appears short, as does the Sagittarius–Carina arm which crosses the local Orion spur where the Sun sits.

Xu et al. (2013) showed a slightly different pitch angle for the Sagittarius and Perseus arms (their Figure 10, about 14°) than for the local Orion arm spur (their Figure 11, about 10°). Their defined spurs have a large pitch angle near 60°, whereas branches have a small pitch angle (<20°). They conclude that the local arm is a branch. It is not a major or minor spiral arm.

REFERENCES

Bodaghee, A., Tomsick, J. A., Rodriguez, J., & James, J. B. 2012, ApJ, 744, 198
Bronfman, L. 1992, Molecular Clouds and Young Massive Stars in the Galactic Disk (Astrophysics and Space Science Library, Vol. 180; Dordrecht: Kluwer), 131
Bronfman, L. 2008, Ap&SS, 313, 81
Camargo, D., Bica, E., & Bonatto, C. 2013, MNRAS, 432, 3349
Camargo, D., Bonatto, C., & Bica, E. 2012, MNRAS, 423, 1940
Caswell, J. L., Fuller, G. A., Green, J. A., et al. 2011, MNRAS, 417, 1964
Chené, A.-N., Borissova, J., Bonatto, C., et al. 2013, A&A, 549, A98
Dame, T. M., & Thaddeus, P. 2008, ApJL, 683, L143
Dame, T. M., & Thaddeus, P. 2011, ApJL, 734, L24
Dobbs, C. L., & Burkert, A. 2012, MNRAS, 421, 2940
Eden, D. J., Moore, T. J., Morgan, L. K., Thompson, M. A., & Urquhart, J. S. 2013, MNRAS, 431, 1587
Effenberger, F., Fichtner, H., Scherer, K., & Busching, I. 2012, A&A, 547, A120
Ellsworth-Bowers, T. P., Glenn, J., Rosolowsky, E., et al. 2013, ApJ, 770, 39
Francis, C., & Anderson, E. 2012, MNRAS, 422, 1283
Grabelsky, D. A., Cohen, R. S., Bronfman, L., & Thaddeus, P. 1988, ApJ, 331, 181
Green, J. A., Caswell, J. L., McClure-Griffiths, N. M., et al. 2011, ApJ, 733, 27
Green, J. A., McClure-Griffiths, N. M., Caswell, J. L., Robishaw, T., & Harvey-Smith, L. 2012, MNRAS, 425, 2530
Griv, E., Ngeow, C.-C., & Jiang, I.-G. 2013, MNRAS, 433, 2511
Han, J. L. 2013, in IAU Symp. 291, Neutron Stars and Pulsars: Challenges and Opportunities after 80 Years, Pulsars as Excellent Probes for the Magnetic Structure in Our Milky Way, ed. J. van Leeuwen (Cambridge: Cambridge Univ. Press), 223
Helminiak, K. G., Devor, J., Minniti, D., & Sybilski, P. 2013, MNRAS, 432, 2895
Higdon, J. C., & Lingenfelter, R. E. 2013, ApJ, 775, 110
Honma, M., Nagayama, T., & Hirota, T. (VERA projects members) 2012, in IAU Symp. 287, Cosmic Masers—from OH to H0, Maser Astrometry with VERA and Galactic Structure, ed. R. S. Booth, E. M. L. Humphreys, & W. H. T. Vilemmings (Cambridge: Cambridge Univ. Press), 386
Jones, C., & Dickey, J. M. 2012, ApJ, 753, 62
Junqueira, T. C., Lépine, J. R., Braga, C. A., & Barros, D. A. 2013, A&A, 550, A91
Kaltcheva, N. T., & Golev, V. K. 2012, PASP, 124, 128
Kharchenko, N. V., Piskunov, A. E., Schilbach, E., Roser, S., & Scholz, R.-D. 2012, A&A, 543, A156
Lopez-Corredoira, M., Cabrera-Lavers, A., Mahoney, T. J., et al. 2007, AJ, 133, 154
Louie, M., Koda, J., & Egusa, F. 2013, ApJ, 763, 94
Majaess, D. J., Turner, D. G., & Lane, D. J. 2009, MNRAS, 398, 263
Matsumoto, N., & Honma, M. (VERA project members) 2012, in IAU Symp. 287, Cosmic Masers—from OH to H0, The Bar Effect in the Galactic Gas Motions Traced by 6.7 GHz Methanol Maser sources with VERA, ed. R. S. Booth, E. M. L. Humphreys, & W. H. T. Vilemmings (Cambridge: Cambridge Univ. Press), 419
Moore, T. J., Urquhart, J. S., Morgan, L. K., & Thompson, M. A. 2012, MNRAS, 426, 701
Nice, D. J., Altiere, E., Bogdanov, S., et al. 2013, ApJ, 772, 50
Pandian, J. D., & Goldsmith, P. E. 2007, ApJ, 669, 435
Piskunov, A. E., Kharchenko, N. V., Roser, S., Schilback, E., & Scholz, R.-D. 2006, A&A, 445, 545
Raddi, R., Drew, J. E., Fabregat, J., et al. 2013, MNRAS, 430, 2169
Roberts, W. W. 1975, VA, 19, 91
Robitaille, T. P., Churchwell, E., Benjamin, R. A., et al. 2012, A&A, 545, A39

Roman-Duval, J., Jackson, J. M., Heyer, M., Tathborne, J., & Simon, R. 2010, ApJ, 723, 492
Sawada, T., Hasegawa, T., Sigimoto, M., Koda, J., & Handa, T. 2012, ApJ, 752, 118
Schnitzeler, D. H. 2012, MNRAS, 427, 664
Siebert, A., Famaey, B., Binney, J., et al. 2012, MNRAS, 425, 2335
Silva, M. D., & Napiwotzki, R. 2013, MNRAS, 431, 502
Steiman-Cameron, T. Y., Wolfire, M., & Hollenbach, D. 2010, ApJ, 722, 1460
Urquhart, J. S., Figura, C. C., Moore, T. J., et al. 2014, MNRAS, 437, 1791
Urquhart, J. S., Hoare, M. G., Lumsden, S. L., et al. 2012, MNRAS, 420, 1656
Urquhart, J. S., Moore, T. J., Schuller, F., et al. 2013, MNRAS, 431, 1752
Vallée, J. P. 1995, ApJ, 454, 119 (Paper I)
Vallée, J. P. 2002, ApJ, 566, 261 (Paper II)
Vallée, J. P. 2005, AJ, 130, 569 (Paper III)
Vallée, J. P. 2008, AJ, 135, 1301 (Paper IV)
Vallée, J. P. 2011, NewAR, 55, 91
Vallée, J. P. 2013, IJAA, 3, 20 (Paper V)
Velusamy, T., Langer, W. D., Pineda, J. L., & Goldsmith, P. F. 2012, A&A, 541, L10
Xu, Y., Li, J. J., Reid, M. J., et al. 2013, ApJ, 769, 15
Zhang, B., Reid, J. J., Menten, K. M., et al. 2013, ApJ, 775, 79